LQG FLUTTER CONTROL OF WIND TUNNEL MODEL USING PIEZO-CERAMIC ACTUATOR

Tatsunori Kaneko* and Yasuto Asano*
*** Department of Mechanical Engineering,**
University of Fukui, Fukui, Japan

Keywords: *Flutter, LQG control, Piezo-ceramic Actuator*

Abstract

A single element of piezo ceramics is used in this study, instead of conventional actuators such as a hydraulic actuator or electric motor, as an actuator in order to control flutter. This study aims at confirming that the free vibration in the still air and the flutter in the wind tunnel, of an aluminum plate wing, can actually be controlled by a single element of a piezo-ceramic actuator by LQG control. The wing model of a rectangular aluminum plate (270.0 mm × 90.0 mm × 0.5 mm) and the aluminum's additional mass (20.0 mm × 150.0 mm × 0.5 mm) has one piezo ceramic element PZT (40.0 mm × 20.0 mm × 0.1 mm) attached on its one side. First we used proportional control for free vibration and flutter in order to confirm the fundamental effectiveness of PZT. And used LQG control for flutter in order to confirm a better effect of PZT. So piezo-ceramic actuator was confirmed to be effective enough to control flutter and confirmed to flutter speed increased.

1 Introduction

Recently, research of the active control technology for flying qualities improvement is advanced in many countries. In active flutter control research control surface is mainly used as an actuator. Piezo-ceramics has small size and lightweight so that it can install in a small place suitable for a sensor/actuator. Therefore, its application to sensing the oscillation and controlling the vibration of structures will increase rapidly in future.

Kawai used the piezo ceramics, instead of a hydraulic actuator or electric motor, as an actuator for making the flutter control actively [1]. In this study we tried to improve his work paying attention to electric force characteristics of a piezo-ceramic actuator. It is assumed that a wing model is composed of an aluminum flat board for fundamental study. We construct mathematical model of a wing model and analytically estimate at how much wind velocity flutter occurs and compare it with experimental value. We obtain aerodynamic forces acting on wing surface by Doublet Point Method [2]. Based on the mathematical model, we design the control law for controlling flutter applying LQG method. We confirm whether we can control flutter by an experiment. We also confirm how much flutter velocity will increase from open loop to closed loop system.

2 Flutter Control Model

A wing model used in the vibration control tests is an aluminum plate wing shown in Fig. 1. The

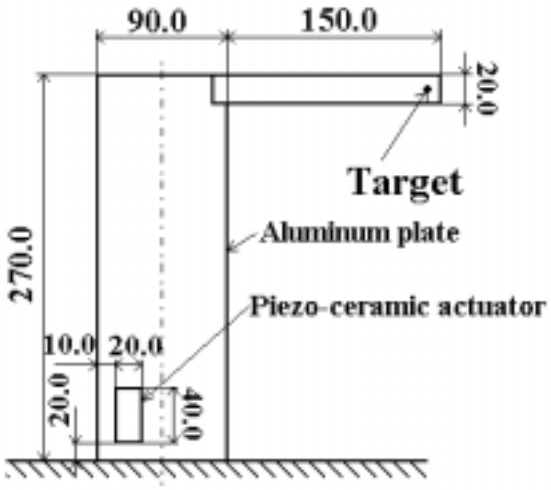

Fig. 1. PZT actuator placed on a model wing spar

wing model of aluminum plate whose aspect ratio is 3 has a single piezo-ceramic element PZT attached on its one side. The size of the aluminum rectangular plate was determined as 270.0 mm × 90.0 mm × 0.5 mm and the aluminum's additional mass was determined as 20.0 mm×150.0 mm×0.5 mm as shown in Fig.1 considering the sectional size of the wind tunnel outflow of 300 mm×300 mm square and the maximum wind speed of 25m/s.

2.1 PZT Actuator

In order to control free vibration and flutter by imposing the strain produced by voltage to the aluminum plate wing model large surface strain for PZT is needed. Piezoelectric relation of PZT attached at wing model is shown in Fig. 2. The surface strain x for PZT is defined by piezoelectric charge constants d_{ij} and an electric field strength E_i as:

$$\begin{Bmatrix} x_1 \\ x_2 \\ x_3 \\ x_4 \\ x_5 \\ x_6 \end{Bmatrix} = \begin{bmatrix} 0 & 0 & d_{31} \\ 0 & 0 & d_{31} \\ 0 & 0 & d_{33} \\ 0 & d_{15} & 0 \\ d_{15} & 0 & 0 \\ 0 & 0 & 0 \end{bmatrix} \begin{Bmatrix} E_1 \\ E_2 \\ E_3 \end{Bmatrix} \quad (1)$$

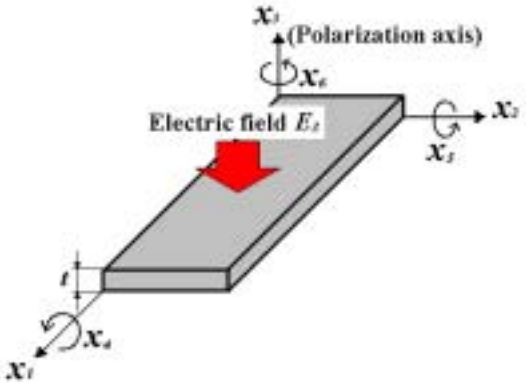

Fig. 2. Piezoelectric relation of PZT

where strain x_4, x_5 and x_6 is sharing strain of rotation of 1 axis, 2 axis and 3 axis.

The direction of polarization is toward x_3 axis since we make use of distortion along the x_1 and x_2 axis. Electric field strength is expressed by the imposed voltage V by $E = V/t$ and the surface strain x can be expressed as follows.

$$\begin{Bmatrix} x_1 \\ x_2 \end{Bmatrix} = d_{31} \frac{V}{t} \quad (2)$$

Since the large surface strain is desirable for PZT, piezoelectric charge constants d_{31} should be large and thickness t should be small. Young's modulus E should be large in order to get a large exerted force. Therefore, PZT of the material properties shown in table 1 was selected and the size of PZT was determined as $40.0mm \times 20.0mm \times 0.1mm$. We used a laser displacement sensor to measure the displacement of a wing tip. The position to measure is shown as a target in Fig. 1 where bending as well as torsion deformation can be detected.

Table 1. Physical constants of PZT at normal temperature

PZT characteristics	Constant
Density	8.1×10^{3} kg/ m^3
Dielectric constants	4900
Piezoelectric charge constants	-375×10^{-12} m/V
Young's modulus	6.4×10^{10} N/m^2
Poisson's ratio	0.32

For simplicity and as a challenge, we decided to use only a single element of PZT. PZT actuators can excite simple bending, simple torsion deformation, or those combinations to the aluminum plate depending on the position and the direction of the actuators. The amount of deflection also depends on them. The position and the direction were determined such that both bending and torsion can be excited and deflection can be as large as possible. Figure 3 shows the actual arrangement of PZT on the aluminum plate. Important restriction of input voltage imposed to PZT is that it should be positive in order to prevent depolarization of PZT.

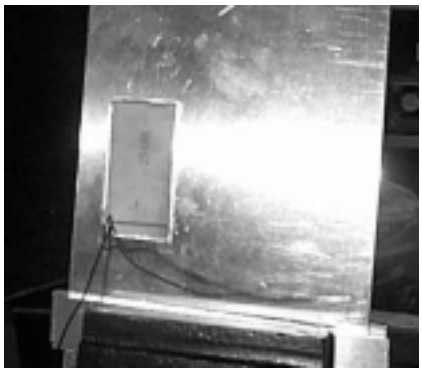

Fig. 3. Aluminum wing model with PZT attached

2.2 Vibration Characteristics of Wing Model

In order to obtain natural frequencies and mode shapes of the wing model, we performed finite element method structural analysis. The finite element model used in analysis is shown in Fig. 4. In this figure, the wing is fixed at the bottom. In analytical result, the first two natural frequencies and mode shapes are shown in Fig. 5. Natural frequencies of a bending dominant first mode and a torsion dominant second mode are 4.62Hz and 11.5Hz, respectively.

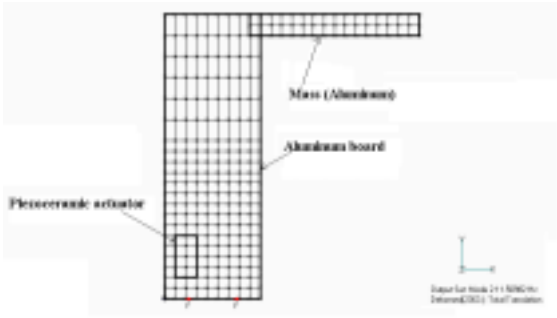

Fig. 4. Finite Element Model

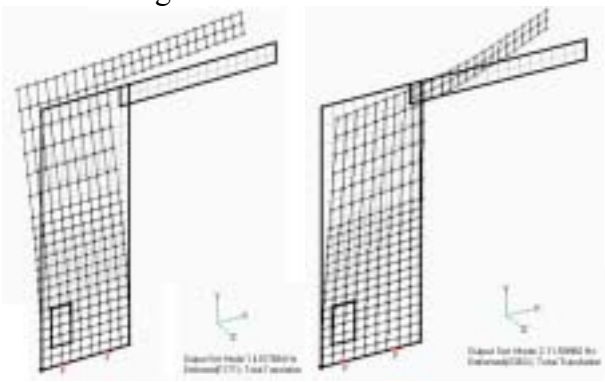

(a) Mode 1 4.62 HZ (b) Mode 2 11.5 Hz

Fig. 5. Mode shape and natural frequency

3 Proportional Control experiments

The free vibration and flutter control test were performed with the test set-up shown in Fig. 6. This test composition is a single input single output system since only single element of PZT actuator is attached on the aluminum plate. The displacement of wing tip is measured by laser displacement sensor and this signal is taken in the AD converter board incorporated the personal computer through charge amplifier. A sampling frequency is 1kHz. The signal output from DA converter board is amplified 24 times with power amplifier, and is imposed on PZT actuator. Maximum-output voltage is 240V.

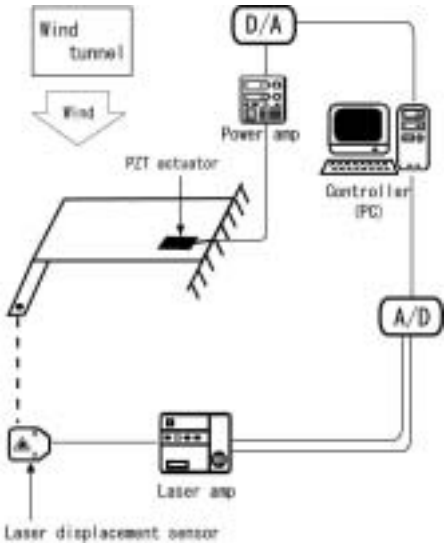

Fig. 6. Schematic diagram of the test set-up

3.1 Control of Free Vibration

We used proportional control for free vibration in order to confirm the fundamental effect of PZT actuator. When the free end of a wing model was flipped by hand, the time response when not performing proportional control is shown in Fig. 7(a), while the time response when performing control is shown in Fig. 7(b).

The control here uses positive voltage alone in order not to loose the piezo-electric effect of PZT, which is so-called control of one-sided effect. With a bias added in PZT and performing linear control is shown in Fig. 7(c). Figure 7(b) and Figure 7(c)(with a bias added)

shows the time response of the proportional control,

$$u = -Ky \tag{3}$$

where the displacement y [mm] is feed back to the PZT command signal u [V] with the proportional gain K [V/mm].

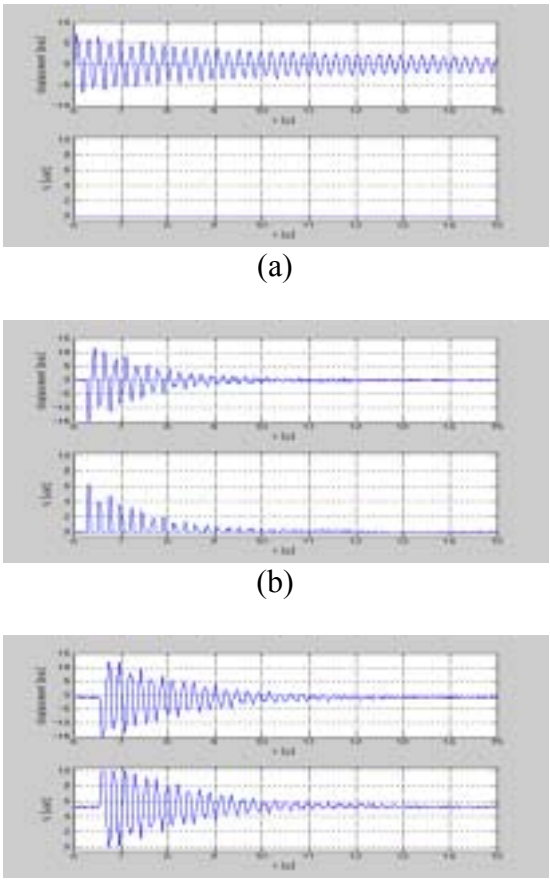

(a)

(b)

(c)

Fig. 7. Time response for proportional control of free vibration

We compared damping characteristics of the system without control and with performing control. The damping has increased greatly by vibration control with the PZT actuator. Though we tried to add a bias voltage to control signal, control effect was not improved so much for this free vibration control.

3.2 Flutter Experiments

For the flutter control experiment was used following small wind tunnel (blow-down type) which is shown in Fig. 8.

Fig. 8. Wind tunnel and position of wing model

Comparison of the response before flutter and during flutter is shown in Fig. 9. The time domain is shown in Fig. 9(a), while the frequency domain is shown in Fig. 9(b), and the response before flutter is shown in Fig. 9(1), while during flutter is shown in Fig. 9(2). In time domain, vibration of bigger amplitude than before flutter has occurred at flutter. The amplitude of flutter is about 6 times larger than the amplitude before flutter and is continuously at constant value. In frequency domain, the bending mode and the torsion mode can be distinguished yet before flutter. When flutter occurs, two frequencies have merged.

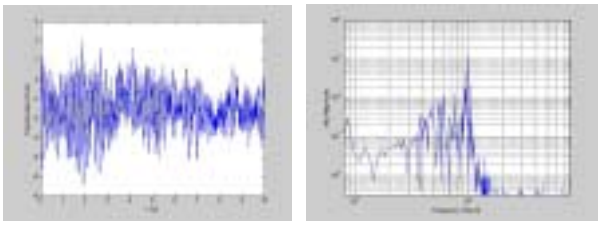

(a) Time domain (b) Frequency domain

Fig. 9 (1) Response just before flutter (wind velocity 13m/s)

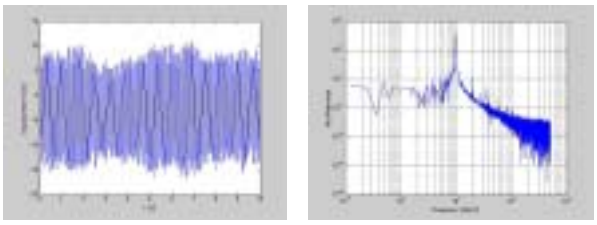

(a) Time domain (b) Frequency domain

Fig. 9 (2) Response during flutter (wind velocity 15m/s)

We performed proportional control of flutter that is shown in Fig 10.

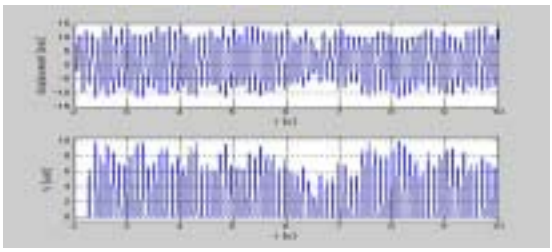

(a)

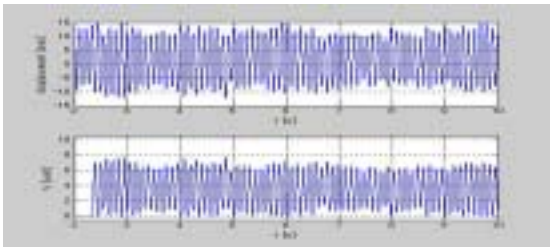

(b)

Fig. 10. Time response for proportional control of Flutter

But there is a control effect neither, we tried to perform control by LQG method.

4 Mathematical Modeling

General dynamic equation of the generalized coordinate $q(t)$ of the wing model on PZT actuator is given in the next expression.

$$M\ddot{q}(t) + C\dot{q}(t) + Kq(t) = f_a(t) + f_p(t) + w(t) \quad (4)$$

Where M , C , K are generalized mass, generalized dumping, and generalized elasticity matrices, respectively. $F_a(t)$, $f_p(t)$ and $w(t)$ are generalized aerodynamic forces term, generalized forces of PZT actuator acting on the wing model, and white noise entered in PZT actuator, respectively. The generalized forces of PZT is assumed here to proportional to the imposed voltage $d_c(t)$ as,

$$f_p(t) = Pd_c(t) \quad (5)$$

The system configuration is a single input-single output system since only single element of PZT actuator is attached on the aluminum plate. We have built a mathematics model of model wing based on FEM analysis followed by Doublet Point Method for aerodynamic analysis. The state space equation takes the following general form.

$$\dot{x}(t) = Ax(t) + Bu(t) + Gw(t) \quad (6)$$

where the matrices in the above equation are,

$$A = \begin{bmatrix} I & 0 & 0 \\ 0 & (M - A_2)^{-1} & 0 \\ 0 & 0 & I \end{bmatrix} \begin{bmatrix} 0 & I & 0 \\ -(M - A_0) & -(C - A_1) & I \\ B_0 & 0 & \Lambda \end{bmatrix}$$

$$B = \begin{bmatrix} I & 0 & 0 \\ 0 & (M - A_2)^{-1} & 0 \\ 0 & 0 & I \end{bmatrix} \begin{bmatrix} 0 \\ P \\ 0 \end{bmatrix}$$

$$G = \begin{bmatrix} 0 \\ -(M - A_2)^{-1} \\ \end{bmatrix} \quad (7)$$

and where A_2, A_1, A_0, B_0 and Λ =diag(- λ ,…,- λ) are coefficient matrices of the following finite dimensional aerodynamic model.

$$\begin{aligned} f_a &= A_2\ddot{q} + A_1\dot{q} + A_0 q + z \\ \dot{z} &= \Lambda z + B_0 q \end{aligned} \quad (8)$$

Output equation of the displacement of the wing tip can be expressed as,

$$y(t) = cx(t) + v(t) \quad (9)$$

where $v(t)$ is a white noise entering in the laser displacement sensor.

4.1 Parameter identification of the structural model

Since we have constructed a mathematical model for the wing, we can identify the structural parameters in the equation of motion for the model. We expected vibration tests to get a frequency response of the wing. The frequency response when we changed frequency of sine wave with 0.5 Hz step is shown in blue lines in fig. 11. We imposed a voltage of a sine wave to PZT and measured the wing response by a laser displacement sensor at a wing tip target. Based on the frequency response, we can get all the parameters in the mathematical model, generalized mass, generalized damping, generalized elasticity, as well as eigen frequencies and eigen modes for the vibration modes of the model in still air. From now on, we will confine ourselves to two modes system retaining only first two modes because flutter occurred in the model can well be expressed with these two modes.

Assuming the linearity for the structural characteristics comprised of a PZT, input voltage $d_c(t)$ imposed on PZT actuator and the generalized coordinate $q(t)$ can be expressed in the following formula.

$$d_c(t) = d_c e^{i\omega t} \tag{10}$$

$$q(t) = \begin{bmatrix} q_{10} \\ q_{20} \end{bmatrix} = \begin{bmatrix} q_{10} e^{i\omega t} \\ q_{20} e^{i\omega t} \end{bmatrix} \tag{11}$$

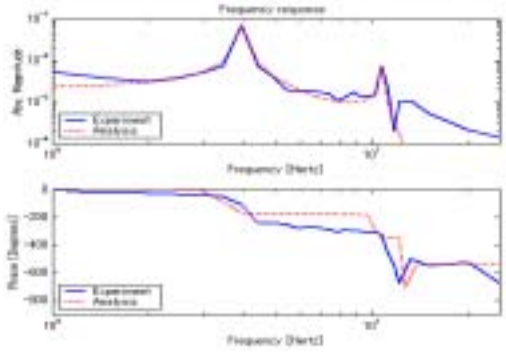

Fig. 11. Frequency response for parameter identification

Substituting the above expressions into eqs. (4), (10) and (11), we can get the following relationship between the amplitudes and eigen frequencies ω_1, ω_2 including damping coefficients ζ_1, ζ_2.

$$-\omega^2 q_{10} + 2i\omega\zeta_1\omega_1{}^2 q_{10} + \omega_1{}^2 q_{10} = \frac{P_1}{m_1} d_{c0} - \omega^2 q_{20} + 2i\omega\zeta_2\omega_2 q_{20} + \omega_2{}^2 q_{20} + \frac{P_2}{m_2} d_{c0} \tag{12}$$

$$-\omega^2 q_{20} + 2i\omega\zeta_2\omega_2 q_{20} + \omega_2{}^2 q_{20} + \frac{P_2}{m_2} d_{c0} \tag{13}$$

Deflection of the wing y(t) at the target of sensor can also be expressed accordingly as,

$$y(t) = y_0 e^{i\omega t} \tag{14}$$

by harmonic vibration. And the amplitude of the wing becomes

$$y_0 = f_1(x_0, y_0) q_{10} + f_2(x_0, y_0) q_{20} \tag{15}$$

Therefore, transfer function comprised by the state space equation takes the form:

$$\frac{y_0}{d_{c0}} = \frac{\frac{P_1}{m_1} f_2(x_0, y_0)}{-\omega^2 + 2i\omega\zeta_1\omega_1 + \omega_1{}^2} + \frac{\frac{P_2}{m_2} f_2(x_0, y_0)}{-\omega_2 + 2i\omega\zeta_2\omega_2 + \omega_2{}^2} \tag{16}$$

Identifying the parameters in eq (16) by the data obtained from a ground vibration test, we could get the following parameters as shown in Fig. 11; the natural frequency of mode 1, mode 2 are ω_1=4.50 Hz, ω_2=10.2 Hz, and the amplitude of mode shapes are $f_1(x_0,y_0)$=1.1824 and $f_2(x_0,y_0)$=0.1216, respectively. The other parameters identified are ζ_1=0.0175, ζ_2=0.007, P_1/m_1=0.5 and P_2/m_2=-2.05.

4.2 Construction of finite dimensional aerodynamic model

Having identified the structural parameters, we have analyzed generalized unsteady aerodynamics using Doublet Point Method. Figure 12 shows the analytical results for 2×2 elements. The aerodynamic matrices can be obtained by least square fitting the analytical results with a finite dimensional model. Fitting has succeeded in getting a model as shown in

Fig. 12. The resulting non-dimensional aerodynamic coefficient matrices, $\hat{A}_2, \hat{A}_1, \hat{A}_0, \hat{B}_0$ are shown below,

$$\hat{A}_2 = \begin{bmatrix} -7.5146e+4 & 0.4459e+4 \\ 0.9739e+4 & -5.072e+4 \end{bmatrix} \quad (17a)$$

$$\hat{A}_1 = \begin{bmatrix} -1.297e+5 & -0.7933e+5 \\ 1.138e+5 & -1.136e+5 \end{bmatrix} \quad (17b)$$

$$\hat{A}_0 = \begin{bmatrix} -0.2122e+5 & -1.453e+5 \\ 0.2098e+5 & -1.365e+5 \end{bmatrix} \quad (17c)$$

$$\hat{B}_0 = \begin{bmatrix} 1.202e+3 & -4.316e+3 \\ -1.343e+3 & 4.718e+3 \end{bmatrix} \quad (17d)$$

Using the above nondimensional matrices, finite dimensional aerodynamic model, eq. (8) can be expressed as the following equation.

$$f_a = \frac{1}{2}\rho U^2 b^2 \left\{ (\frac{b}{U})^2 \hat{A}_2 \ddot{q} + (\frac{b}{U}) \hat{A}_1 \dot{q} + \hat{A}_0 q + z_r \right\} \quad (18)$$

$$(\frac{b}{U})\dot{r} = \Lambda r + \frac{1}{2}\rho U^2 b^2 \hat{B}_0 q \quad (19)$$

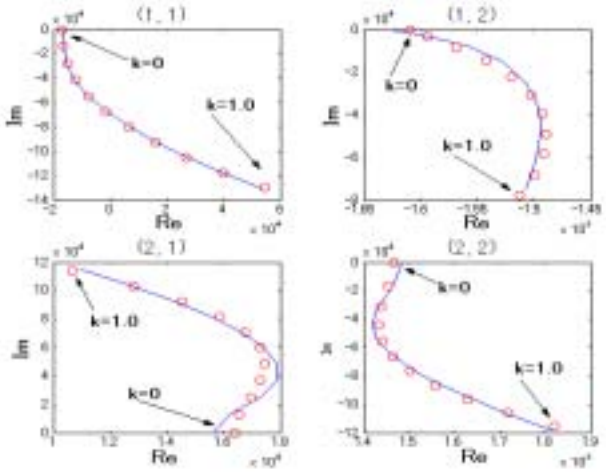

Fig. 12. Generalized aerodynamic coefficients and finite state model fitting

where ρ is air density, U is airflow velocity and 2b is a mean chord length.

5 LQG Control Design

Having constructed a finite state aeroelastic model, we can obtain the flutter characteristics in the form of root locus in airspeed. Incorporating the velocity-dependent characteristics in the aerodynamic forces expressed in eq. (18), we can get the eigen value variation with an airspeed as a root locus.

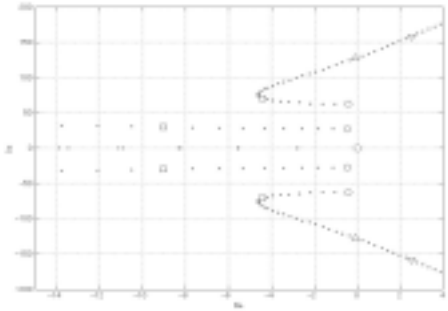

Fig. 13. Wind velocity root locus of the open loop system

Actually, a branch starting from the second (torsion) mode behaves rather strange. Instead of decreasing the frequency as the velocity, it increases its frequency and coupling is not realized with the first (bending) mode. Though at present moment, we only have checked that the change of the sign in static aerodynamic force in torsion mode can influence this coupling, we have not yet found any decisive reason of this phenomenon.

We have continued to design an output feedback by LQG method. By applying the LQG method, we have obtained the following control laws that comprises regulator with estimated states $\hat{x}(t)$ by Kalman filter.

$$\dot{\hat{x}}(t) = A\hat{x}(t) + Bu(t) + K_2\{y(t) - c\hat{x}(t)\} \quad (20)$$

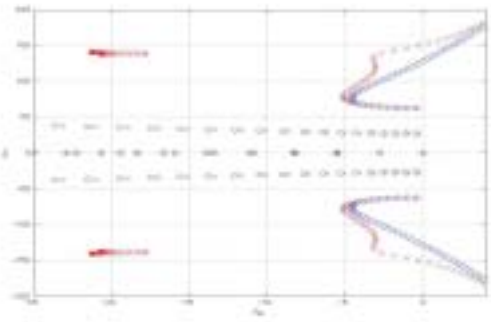

Fig. 14. Wind velocity root locus of the closed loop system for LQG controller (○: open loop, ×: closed loop)

$$u(t) = -K_1 \hat{x}(t) \qquad (21)$$

Eigen value analysis was carried out for a closed loop system and figure 14 shows a wind velocity root locus of a closed loop system compared with an open loop system. The results show that the flutter velocity 15.0 m/s predicted for an open loop system is increased to 18.25 m/s with 21.7 % increasing.

6 Flutter Control Wind Tunnel Experiment

Wind tunnel tests were performed to verify the control law effectiveness. We first checked the frequency change of two modes that may contribute flutter according to velocity change. Figure 15 shows the results that show the coalescence of two modes. Flutter speed without control is estimated as 12.3 m/s.

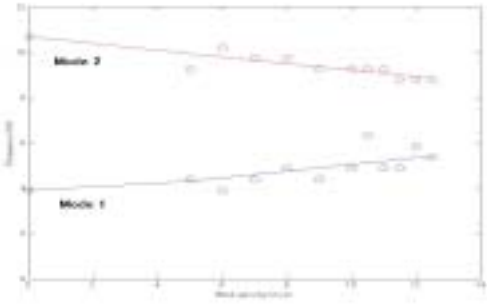

Fig. 15. Frequency coalescence of two modes

The control law designed by LQG method based on a mathematical model expressed in eq. (6) and showing unique trend of frequency was installed in PC. The flutter was suppressed by the control as shown in Figure 16. When LQG controller is applied, flutter speed is increased to 12.8 m/s, i. E., 4.0 % increase. Since the predicted increase of flutter speed is 21.7 %, the actual increase is not sufficient. Possible cause of the discrepancy may exist in insufficiency in the mathematical model.

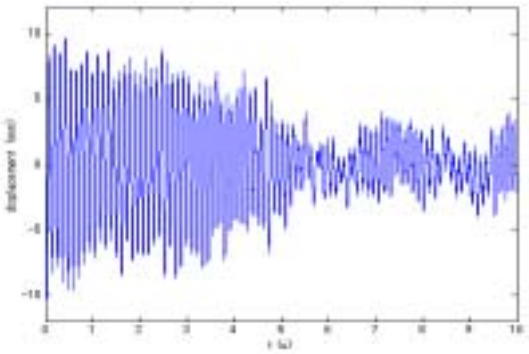

Fig. 16. Wind tunnel test data for successful flutter suppression by PZT

7 Conclusions

We examined a free vibration control, flutter proportional control and LQG flutter control using piezo ceramic actuator. In case of flutter control we examined the effect of intentional shift that moves an equilibrium state to positive state (bias). In the result, flutter can be controlled better by a linear control with a bias added than a non-linear control of a one-sided effect. Since the increment of the flutter velocity in the test was not enough compared with the analytical prediction, improvement of the mathematical model is necessary in future work.

References

[1] Kawai, N., "Flutter Control of Wind Tunnel Model Using a Single Element of Piezo-Ceramic Actuator," Proceedings of the 24th International Congress of the Aeronautical Sciences, Yokohama, Japan, 5.7.3.1-5.7.3.6, 2004

[2] Ueda, T. and Dowell, E. H., "A New Solution Method for Lifting Surfaces in Subsonic Flow," AIAA Journal, vol. 20, March 1982, pp. 348-355.